METEOROLOGICAL APPLICATIONS
Meteorol. Appl. **25**: 40–48 (2018)
Published online 18 August 2017 in Wiley Online Library
(wileyonlinelibrary.com) DOI: 10.1002/met.1667

Future extreme rainfall change projections in the north of Iran

Reza Modarres,* Mohammad Ghadami, Sohrab Naderi and Mohammad Naderi
Department of Natural Resources, Isfahan University of Technology, Iran

ABSTRACT: Future changes in extreme rainfall arising from climate change may have a significant influence on flood and water erosion control and management strategies to a great extent. The maximum daily rainfall time series were projected for 2020–2049 using six general climate models and two scenarios through artificial neural networks for 22 stations across the north of Iran. The results indicate a reduction of between −3.0 and −0.2% in maximum rainfall for the selected stations and five out of six of the general climate models. The changes in the frequency and magnitude of extreme rainfall were then investigated by fitting a generalized extreme value distribution to the historical (from 1981 to 2010) and projected maximum rainfall. The location parameter of the generalized extreme value distribution fitted to the projected maximum rainfall does not show a significant change while the scale and shape parameters exhibit significant changes compared to the historical period. Estimating the 2, 50 and 100 year return periods showed that the maximum rainfall will have a reduction in the probability of large amounts across the region compared with the base period while the number of extraordinary extreme events may show growth. As a region vulnerable to flash floods and water erosion due to rainfall characteristics and land use change from forest to agriculture, the results may send an alarm to define long term and effective strategies for future flood control management in the region.

KEY WORDS climate change; extreme rainfall; artificial neural network; downscaling; GEV distribution; Iran

Received 12 November 2016; Revised 28 January 2017; Accepted 2 March 2017

1. Introduction

During the last decade, changes in the frequency and magnitude of extreme rainfall events under the impact of climate change or anthropogenic consequences have attracted substantial attention (e.g. Alexander *et al*., 2006; Tryhorn and DeGaetano, 2011; among others). Given that these extreme events have high risk to human health, add uncertainty to policy decisions, and destroy environmental, agricultural, hydrology and water resource infrastructures, projecting their future local or regional scale changes is a crucial task.

The current procedures for projecting climate changes in the near and far future are based on general circulation models (GCMs). GCMs are available for coarse spatial resolutions but are unable to provide information for finer local resolution on the behaviour of hydro-climate variables. This inadequacy is the reason for improving statistical and dynamic downscaling techniques (Sarhadi *et al*., 2016, 2017).

Among statistical downscaling methods, functional relationship-based methods such as multivariate regression methods are popular and easy to use for climate change projections (Huth, 2004; Frost, 2007; Hessami *et al*., 2008; Tumbo *et al*., 2010; Jeong *et al*., 2012a). Since there is a nonlinear interrelationship between climate and hydrological systems, many studies have focused on nonlinear methods for downscaling the behaviour of large atmospheric–oceanic predictors into regional or local predictants such as rainfall, temperature or streamflow time series.

Among different nonlinear models, artificial neural networks (ANNs) are very popular due to their capability for identifying nonlinear spatial and temporal complex patterns in climatic variables. The application of ANNs for statistical downscaling can be seen in many papers. For example, Schoof and Pryor (2001) compared regression and ANN models for temperature and precipitation downscaling in the midwestern United States. They demonstrated the superiority of ANNs in temperature downscaling, while the accuracy of precipitation did not show a significant improvement. Coulibaly and Dibike (2005) proposed time-lagged feedforward neural networks for downscaling of daily total precipitation and maximum and minimum temperature series for the Serpent River watershed in northern Quebec (Canada). Fistikoglu and Okkan (2011) used NCEP/NCAR Reanalysis data to downscale monthly precipitation for the Tahtali River Basin in Turkey through ANNs and achieved the best results from a log-sigmoid function. Jeong *et al.* (2012b) compared ANNs with different transfer functions such as regression models for temperature downscaling and showed that multiple regression for monthly series performs better than an ANN except for the minimum temperature for which the ANN performs better.

One of the results of climate change is a change in the hydrological and climatic extremes in the future. The Intergovernmental Panel on Climate Change (IPCC) in its Fourth Assessment Report (Hegerl *et al.*, 2007) defines extremes as rare events at a particular area and for a specific time. In the context of a climate change effect on extremes, two questions arise: (1) does climate change increase/decrease the magnitude of extreme events in the future, and (2) does climate change increase/decrease the frequency of extreme event occurrences? In this case, there are numerous studies in the literature to project future changes in extreme rainfall using different GCMs and climate change scenarios.

* Correspondence: R. Modarres, Department of Natural Resources, Isfahan University of Technology, PO Box 8415683111, Isfahan, Iran. E-mail: reza.modarres@cc.iut.ac.ir

For example, the future change of two precipitation indices over the Greek area was simulated by ANNs using the HadAM3P model by Tolika *et al.* (2008). For downscaling of maximum and minimum temperature at the Pichola Lake in arid Rajesthan state, India, Goyal and Ojha (2012) used and compared linear regression and ANNs and indicated the superiority of ANNs over the regression method using different statistical criteria. Tue Vu *et al.* (2016) applied a feedforward network to downscale rainfall from three GCM models and showed an increasing trend of precipitation for the rainy season in Bangkok, Thailand. Li *et al.* (2012) showed more frequent and intense precipitation on the Loess plateau in China based on six GCMs and three emission scenarios. Huang *et al.* (2012) simulated extreme precipitation indices across the Yangtze river basin by the statistical downscaling method and found a slight increase in the 2050s and a significant increase in the 2080s.

The aim of this study was thus to project changes in the magnitude and frequency of maximum monthly precipitation in the north of Iran based on ANN downscaling. In the following section, the dataset and methods used for projecting future changes in the magnitude and frequency of extreme rainfall over the study region are presented. The results are then provided and discussed in Section 3. The conclusion of the research is given in Section 4.

2. Datasets and methodology

2.1. Study area and data

The Caspian Sea basin includes the northern hill slopes of the Elburz Mountains and plains of the sea margins in the north of Iran. This area covers more than 170 000 km^2 of the country (11%). The basin has the highest relief in the country, where the maximum and minimum elevations have 5500 m difference. There are 13 major basins with area above 1000 km^2 having different hydro-climatic conditions. These basins vary from mountainous forest to agricultural lowland regions along the Caspian Sea coasts. The region receives the highest amount of precipitation in the country, in the form of rainfall over plains and snow over the mountainous watersheds.

The precipitation pattern in the north of Iran changes from west to east. While the western region receives more than 1000 mm per year on average, the rainfall decreases to less than 300 mm in the eastern part. The western region has the highest amount of rainfall and relative humidity compared with all other parts of the country and experiences summer rainfall, which is not seen for any other region in Iran. In addition, intense rainfall is another typical characteristic of the northern parts of the region, where the concentration index is the highest in the entire country (Alijani *et al*., 2008). These frequent intense rainfall events are therefore an important source of flooding and a massive soil erosion hazard in this region. Characterized by steep hills and watersheds, land use changes and deforestation in recent decades make the region susceptible to destructive flood events. Many flood events are reported each year due to intense extreme rainfall in the region with high return periods (low frequency). These floods have been influencing people's lives and infrastructures along the Caspian Sea margins during recent years. Therefore, it is of crucial importance to investigate any changes in extreme rainfall events to depict the risk of extreme floods in the future and to develop and modify flood control strategies and management.

In this regard, two types of data are used to simulate future changes in maximum rainfall. The first type of data includes historical daily rainfall time series of 22 stations across the study area (Table S1) from 1981 to 2010. From these daily data, 24 h maximum rainfall time series were extracted as the historical data. The spatial distribution of the selected stations over the study area is presented in Figure 1.

2.1.1. *GCM outputs*

GCMs are considered as excellent tools to study long term climate changes by providing current and future global and regional climate variables. This simulation of current and future climate is achieved by various internal and external atmospheric driving factors such as greenhouse gas emissions through different scenarios (Raje and Mujumdar, 2009). GCMs depict the climate of

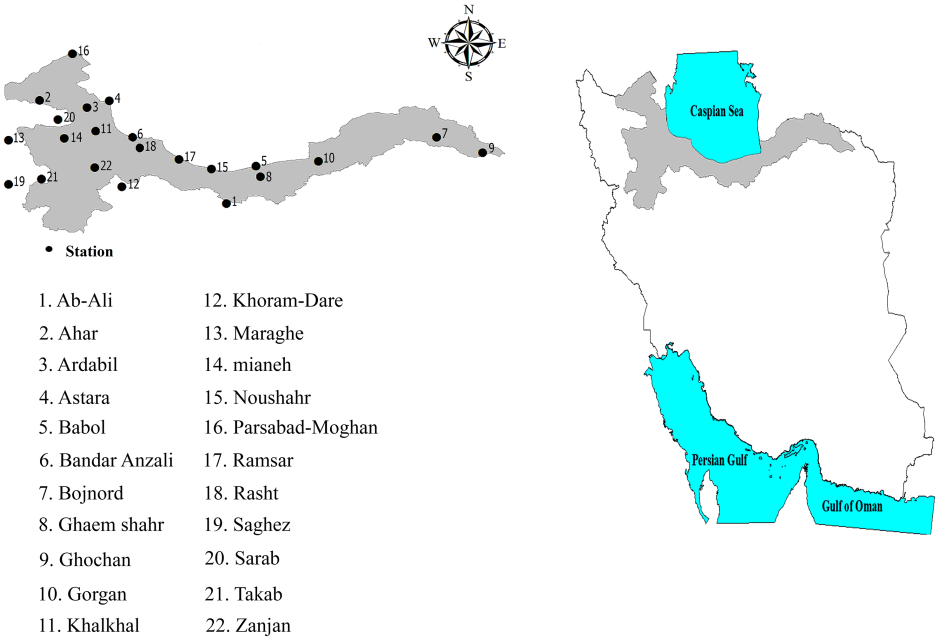

Figure 1. Study area and geographical location of stations across the north of Iran. [Colour figure can be viewed at wileyonlinelibrary.com].

the Earth using a 3D grid with a horizontal resolution of between 250 and 600 km and 10–20 vertical layers in the atmosphere and 30 layers in the ocean (Houghton *et al*., 2001).

The second type of data is the daily climate model outputs for two periods, 1981–2010 as the historical period and 2020–2049 as the near future period.

In this study, rainfall outputs of six GCMs related to the IPCC Fourth Assessment Report and two scenarios, A2 and B1, are used. These two scenarios are widely used for climate change assessment in different studies. The models and their references are given in Table S2. The outputs of the GCMs for the selected stations were obtained from Canadian Climate Data and Scenarios (available at: http://www.cccsn.ec.gc.ca). The detailed information of the prognostic atmospheric and oceanic variables for the selected GCMs is available at http://www.ipcc-data.org. The direct link to the models is presented in Supporting Information.

2.2. Methods

To project future monthly maximum rainfall and its probabilistic behaviour, the next steps are followed.

2.2.1. Artificial neural networks

In this study, to project future maximum rainfall, the daily rainfall is downscaled through ANNs using six GCM outputs.

ANNs are mathematical models which try to resemble brain operation and processes. The use of ANNs in hydrology and climatology has a long history in the literature (McCulloch and Pitts, 1943; ASCE Task Committee on Application of Artificial Neural Networks in Hydrology, 2000). ANNs can be designed to model the relationship between some independent variables as input data and dependent variables as output data through the structure of the ANNs, which includes a series of nodes, neurons and layers.

In this case the interest was to establish a relationship between GCM outputs and historical maximum daily precipitation during 1981–2010. This was followed by training an ANN so that it can replicate the relationship between GCM outputs and historical maximum daily precipitation. For this purpose, the historical dataset was divided into two series; 1981–2000 for ANN calibration (training) and 2001–2010 for ANN validation.

In this study a feedforward multilayer perceptron (MLP) architecture of ANNs was applied. MLPs consist of a number of layers which have several nodes themselves. Each node in a layer has a link to a node in both previous and subsequent layers. For an ANN with n input neurons ($x_1, \ldots, x_n$), h hidden neurons ($w_1, \ldots, w_h$) and m output neurons ($Z_1, \ldots, Z_m$):

$$Z_{k=f}\left(\sum_{j=1}^{h}\alpha_{kj}w_j+\varepsilon_k\right) \qquad k=1,\ldots,m \tag{1}$$

$$w_{j=g}\left(\sum_{i=1}^{n}\beta_{ji}w_i+\tau_j\right) \qquad j=1,\ldots,h \tag{2}$$

where g and f are activation functions, i, j and k represent input, hidden and output layers respectively, τ_j is the bias of neuron w_j, ε_k is the bias of neuron z_k, β_{ij} is the weight of the connection from neuron x_i to w_j and α_{jk} is the weight of the connection from neuron w_j to z_k. The process of determining the weights, 'training' or 'calibration', is carried out based on the observed input and output pattern. The downscaling procedure is provided in Figure S1. Based on the above training and validation steps and developing the best network, the future daily rainfall dataset was projected for 2020–2049.

2.2.2. Generalized extreme value (GEV) distribution

In order to investigate the changes in the frequency distribution of maximum rainfall under climate change, the GEV distribution is fitted to the observed and projected extreme rainfall time series.

The cumulative and probability density function (CDF and PDF) respectively of the GEV distribution are as follows:

$$F(x)=\exp\left(-\left[1-\left\{\frac{k(x-\mu)}{\alpha}\right\}^{\frac{1}{k}}\right]\right) \tag{3}$$

$$f(x)=\alpha^{-1}\exp\{-(1-k)y-\exp(-y)\} \tag{4}$$

and

$$y=-k\log\left\{1-\frac{k(x-\mu)}{\alpha}\right\} \tag{5}$$

where $k\neq 0$. In the above equations, x denotes annual maximum rainfall and μ, σ and k are the location, scale and shape parameters, respectively.

The location parameter indicates the shift of the GEV distribution in a horizontal direction while the scale parameter describes how spread the distribution is and where the bulk of the distribution lies. Therefore, the frequency distribution of the maximum rainfall will spread out if the scale parameter increases. The third parameter describes the shape of the distribution and governs the tail of the GEV distribution. A shape parameter $k=0$ gives an extreme value type I (EVI) or Gumbel distribution, $k>0$ gives an EV2 or Frechet distribution and $k<0$ gives a Weibull distribution.

The negative value of the shape parameter determines that the distribution is upper bounded while a positive shape parameter leads to the GEV distribution being upper bounded and undesirable for practical applications (Millington *et al*., 2011). The aim was to seek changes in the parameters of the GEV distributions of the observed and projected maximum rainfall.

3. Results

Based on the daily rainfall projected by the GCMs, the maximum and average daily rainfall for each month are projected for two scenarios (A2 and B1) and compared with historical data. The percentage changes in the mean maximum rainfall for the two scenarios are illustrated in Tables 1 and 2 for each station and model.

According to scenario A1 (Table 1), the highest changes in the maximum rainfall are projected by the MCM3 model, which shows a positive change (on average). Other models give negative (decreasing) changes in the maximum rainfall. The highest reduction is projected by the ECHAM model (−4.7%) followed by the CGCM model, which indicates a −4.3% reduction in maximum rainfall. On the other hand, the highest positive changes are observed for the Astara and Mianeh stations with 72.5 and 28.7% respectively, which are projected by the MCM3 and CCSM3 models. The highest decrease in maximum rainfall is observed for Astara (−45.5%) and Mianeh (−38.3%) by the BCM and ECHAM models, respectively. The average changes for all the models show a negative tendency for most of the stations in the north of Iran, where Noushahr shows the highest decreasing change (−3.17%) and Mianeh shows the highest positive change (+1.47%). Based on the A1 scenario and all the models, the

Table 1. Percentage change in the maximum rainfall − scenario A2.

Station	BCM	CGCM	MCM3	CSIRO	ECHAM	CCSM3	Average
Ab-Ali	−7.0	4.0	16.0	−10.0	−11.0	−5.0	−2.17
Ahar	−0.8	−10.2	10.2	−1.3	4.0	−8.7	−1.13
Ardabil	−3.4	−0.5	11.0	−15.8	4.2	6.8	0.38
Astara	−45.5	−25.9	72.5	3.7	−8.4	−6.5	−1.68
Babolsar	−3.1	2.0	4.5	−0.6	−3.1	−8.5	−1.47
Bandar Anzali	0.4	−0.7	1.7	−1.6	−3.0	−7.9	−1.85
Bojnord	−8.6	6.5	9.4	−9.4	−6.7	9.6	0.13
Ghaemshahr	−0.4	−1.2	−3.5	2.9	5.9	−10.4	−1.12
Ghochan	0.6	1.3	18.3	−14.9	−3.7	−9.9	−1.38
Gorgan	−1.3	−1.2	3.9	3.7	−7.0	−3.5	−0.90
Khalkhal	1.5	−6.4	12.4	−10.1	−3.5	4.8	−0.22
Khoramdare	−4.7	0.4	8.1	−2.6	−1.1	−8.5	−1.40
Maraghe	6.2	−15.7	26.7	−12.5	−12.1	5.6	−0.30
Mianeh	10.1	−15.0	19.0	4.3	−38.3	28.7	1.47
Noshahr	0.6	−3.8	0.7	9.1	−8.1	−17.5	−3.17
Parsabad	6.5	−4.8	1.8	−2.0	−10.1	4.3	−0.72
Ramsar	−5.7	1.2	0.1	−4.6	1.3	−4.9	−2.10
Rasht	−1.1	−0.6	4.2	−3.5	4.2	−11.6	−1.40
Saghez	10.3	1.7	4.3	6.4	−11.7	−9.6	0.23
Sarab	2.2	−5.7	8.5	−10.7	8.1	3.5	0.98
Takab	5.8	−17.0	14.2	−1.0	−5.6	−8.6	−2.03
Zanjan	0.0	−4.5	12.1	−12.5	2.6	−2.6	−0.82
Average	−1.7	−4.3	11.7	−3.8	−4.7	−2.7	

Table 2. Percentage change in the maximum rainfall − scenario B1.

Station	BCM	CGCM	MCM3	CSIRO	ECHAM	CCSM3	Average
Ab-Ali	−7.0	−2.0	21.0	−11.0	−9.0	5.0	−0.50
Ahar	3.4	−3.7	−1.9	−7.8	13.5	−5.7	−0.37
Ardabil	−5.4	3.4	8.5	−16.3	7.6	9.6	1.23
Astara	−41.9	−26.7	72.9	−3.3	−6.8	1.0	−0.80
Babolsar	−3.1	−0.2	6.7	−2.2	−0.4	−8.5	−1.28
Bandar Anzali	4.0	−7.1	4.2	−2.0	−4.5	−4.8	−1.70
Bojnord	−4.4	3.8	3.1	−4.6	−8.2	11.7	0.23
Ghaemshahr	−4.6	−1.0	−2.2	0.0	6.4	−4.5	−0.98
Ghochan	7.4	−3.9	16.0	−15.1	−4.5	−2.8	−0.48
Gorgan	−4.4	9.4	−2.1	6.1	−7.7	−6.4	−0.85
Khalkhal	4.0	−3.9	6.4	−8.6	−7.7	11.2	0.23
Khoramdare	1.4	−11.3	12.1	−3.6	−0.1	−4.9	−1.07
Maraghe	5.8	−12.5	23.8	−15.9	−7.9	8.4	0.28
Mianeh	17.6	−16.1	12.7	1.3	−34.1	31.9	2.22
Noshahr	0.6	−7.0	1.8	10.4	−7.1	−15.5	−2.80
Parsabad	0.2	3.8	−6.1	1.3	−7.8	6.4	−0.37
Ramsar	−4.7	2.9	−5.6	−0.2	−3.6	−5.1	−2.72
Rasht	−0.5	−4.8	8.3	−8.4	9.6	−7.4	−0.53
Saghez	10.3	−3.7	7.5	−3.2	−3.7	−11.6	−0.73
Sarab	7.9	−8.2	6.6	−12.1	8.7	3.4	1.05
Takab	7.2	−14.9	12.6	−8.8	−2.4	−4.3	−1.77
Zanjan	4.7	−4.7	5.4	−8.2	−1.3	2.3	−0.30
Average	−0.1	−4.9	9.6	−5.1	−3.2	0.4	

average change in maximum rainfall for all stations is −0.94% (about 1%) for the north of Iran.

Based on the results from the B1 scenario (Table 2), the highest positive changes in maximum rainfall are projected by the MCM3 model (on average) and for the Astara and Mianeh stations (similar to the A2 scenario, Table 1). The highest decreasing changes are observed from the BCM and CGCM models in the Astara station (−41.9 and −29.7%). However, the highest negative changes are projected by the CSIRO model (−5.12% on average).

Comparing different stations shows that Mianeh station has the highest positive (2.22%) and Noshahr the highest negative changes (−2.80%) in the future based on different climate models. The average changes in maximum rainfall for all stations and for the B1 scenario seem to be very low (−0.55%) for the study region.

The GEV probability distribution function of the annual maximum rainfall for eight stations is provided in Figure 2. It should be noted that these PDFs of the projected rainfall have been averaged over six GCM outputs. A typical shift to the left is observed in the PDFs illustrating a significant change in the magnitude of the upper tail or high rainfall amounts as well as an increasing probability of medium amounts of maximum rainfall. This figure also shows a reduction in the range of

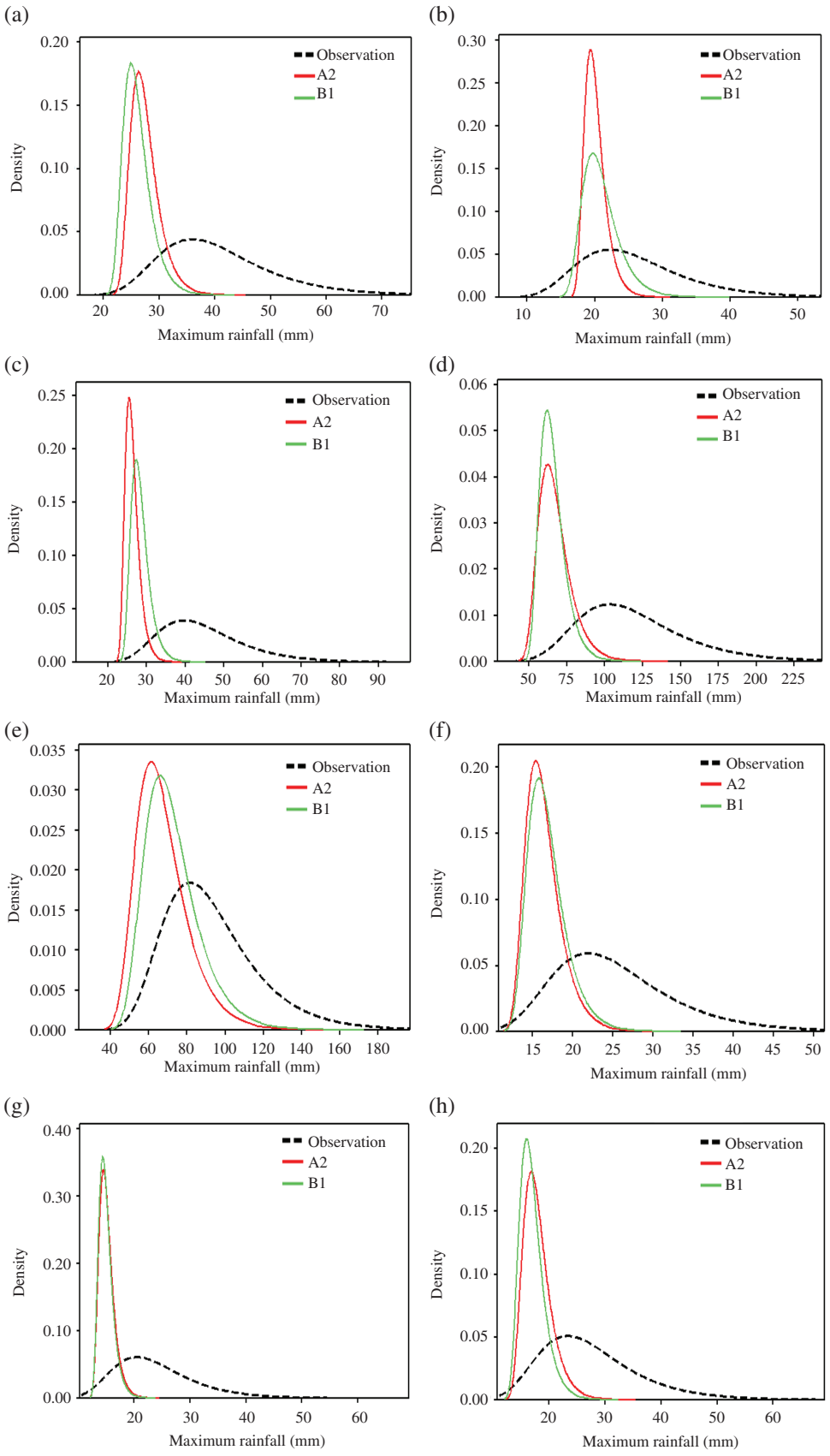

Figure 2. Observed and projected (A2 and B1 scenarios) probability density functions of the annual maximum rainfall for selected stations (a) Ab-ALI, (b) Ghochan, (c) Gorgan, (d) Noshahr, (e) Rasht, (f) Zanjan, (g) Ardabil and (h) Parsabad-Moghan. [Colour figure can be viewed at wileyonlinelibrary.com].

maximum rainfall amount toward average values and increasing peakedness.

Changes in the GEV parameters of the projected extreme rainfall were investigated on a regional scale. The box-whisker plots of these parameters are illustrated in Figure 3 for different GCM models. Each boxplot includes 22 parameters for 22 stations. The changes in the median of the location parameter (μ) are not significant between observed and future extreme rainfall. In addition, the location parameter does not show a large difference between the GCM models as well as the two scenarios. This implies that the changes of the horizontal shift of the location parameter from historical rainfall to future projected rainfall are negligible. However, the change in the scale parameter (σ) shows a remarkable reduction in both median and range based on different climate models for the future. It should also be noted that the two scenarios are almost the same in the scale parameter. This reduction in variance has also been mentioned as a common feature for downscaled rainfall data in other studies such as Jeong *et al.* (2012a, 2013) and Shahriar Pervaz and Henebry

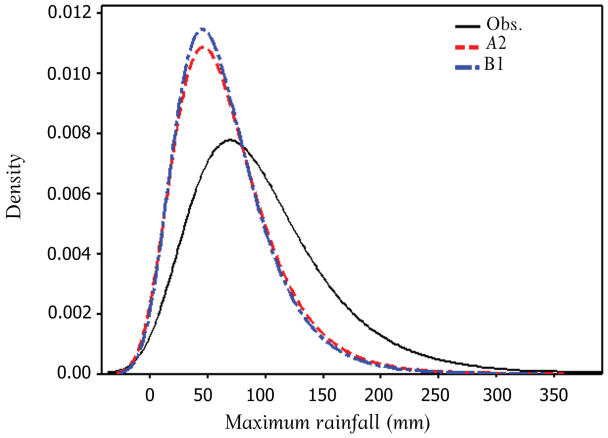

Figure 4. Regional probability distribution function for the annual maximum rainfall across the study area. [Colour figure can be viewed at wileyonlinelibrary.com].

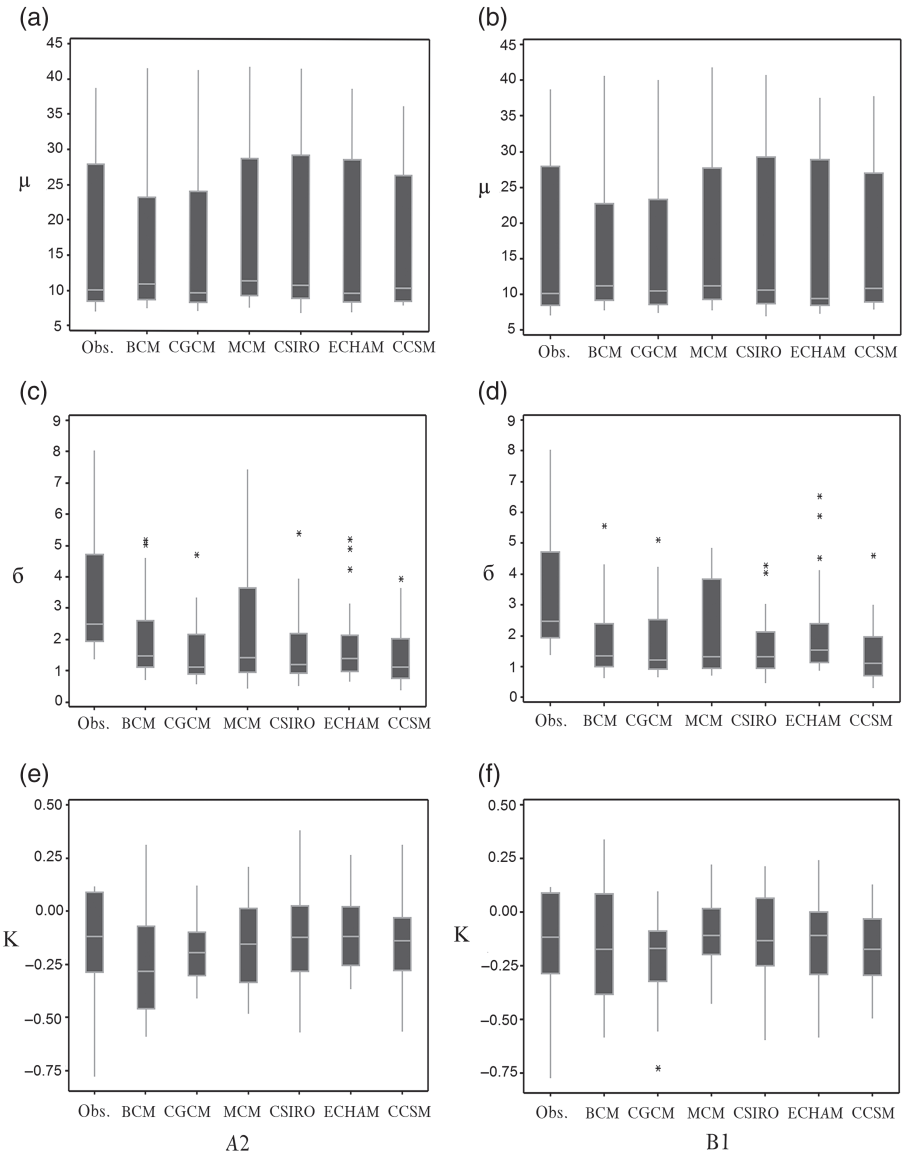

Figure 3. Box-whisker plots of generalized extreme value (GEV) parameters for observed (obs.) and projected (A2 and B1 scenarios) annual maximum rainfall based on two scenarios, A2 (a, c, e) and B1 (b, d, f).

(2014). It should be noted that the above studies have applied a linear transfer function rather than a nonlinear function such as the ANN used in this study.

The shape parameter (k) shows no significant changes in both median and interquantiles (25^{th} and 75^{th} quantiles) for the entire region. It is also interesting to see that the values of the shape parameters remain negative in the future based on the different models indicating the suitability of GEV parameters for fitting to extreme rainfall in the north of Iran in the future.

Additionally, the GEV probability distribution functions of maximum rainfall are provided to investigate the change in the probabilistic behaviour of maximum rainfall. These PDFs are drawn for the entire region. In other words, each PDF includes 22 values taken from each station. More detailed information on the PDFs is also provided in Figure S2.

Figure 4 illustrates the PDFs of the annual maximum rainfall across the north of Iran. It can be seen that the highest density (or the peak of the PDFs) of maximum rainfall tends to remain

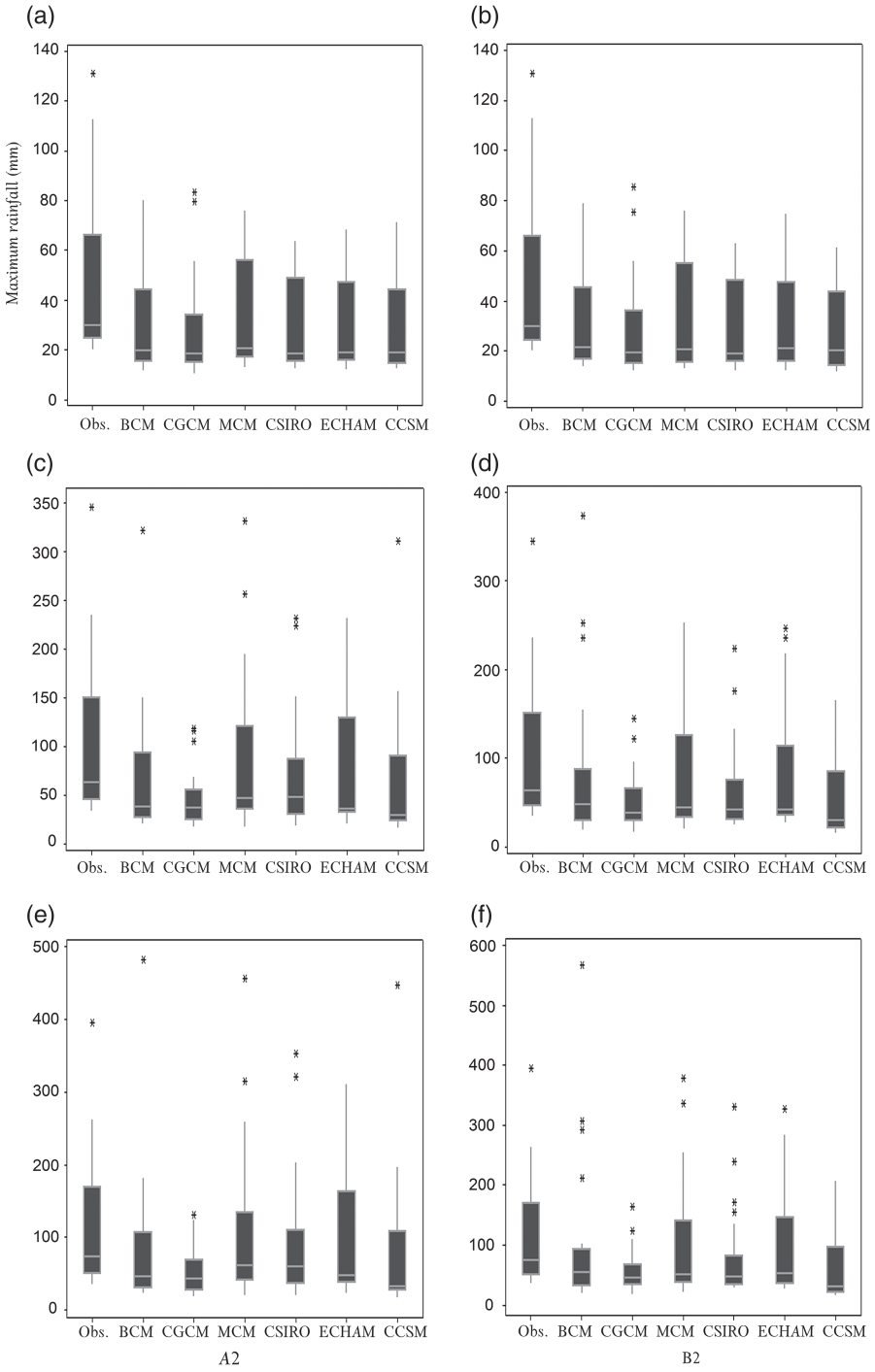

Figure 5. Observed and projected (A2 and B2 scenarios) maximum rainfall in 2-year return period (a–b), 50-year return period (c–d) and 100-year return period (e–f) from six general circulation models.

almost the same (or with a small shift to the left) as observations of the base period for both scenarios and different GCMs on the horizontal axis. This shift to the left is also observed for the values in the right tail of the PDFs where the tail is shifting to the left (or to smaller values of the average maximum) compared with the historical data (1981–2010). This change is also observed for the maximum rainfall with a more remarkable shift. The peakedness of the PDFs has become larger while the range of extreme rainfall has become smaller and the probability of occurrence of extreme rainfall is becoming smaller in the future for all GCMs.

To explore the changes in the rainfall frequency, the maximum rainfall in 2, 50 and 100 year return periods was also estimated based on the GEV distribution. The box-whisker plots of the maximum rainfall for different return periods are given in Figure 5.

It is observed that the median and range of the maximum rainfall decrease in the near future according to all the GCMs across the region. However, the number of extreme (outlier) events increases, especially for 50 and 100 year return periods. These changes in the maximum rainfall may be related to the decrease in the total annual rainfall but the increase in extreme events may show an increasing risk of extreme flood events, with significant potential damage across the northern parts of Iran.

4. Conclusion

Extreme rainfall is a key element in hydrological modelling, erosion and flood control and management worldwide. In this study, artificial neural network based downscaling using six general circulation models showed remarkable changes in the magnitude and probability of extreme rainfall where the average or the median rainfall events will decrease in magnitude but their probability is not changed or shows a slight increase while the magnitude and probability of large events will decrease. However, the number of extreme events (outliers or the upper tail of the generalized extreme value distribution) will increase. This study also indicated the changes in the parameters of the generalized extreme value distribution fitted to maximum rainfall. The location parameter does not show a significant change compared to the historical period, while the scale and shape parameters show a notable change. This can be reflected in the probability density function figures of the maximum rainfall on both at-site and regional scales.

5. Recommendation for future studies

This study provides for the first time a probabilistic picture of changes in extreme rainfall in the north of Iran as a major region with the risk of flood, which can be developed for other regions of the country. However, it is necessary to project future change in the flood frequency occurrences as well in this region to be able to perform better actions in flood and soil erosion control. Although this study was carried out based on six different general circulation models, it is necessary to use other models in order to have a more complete vision about future change in extreme events in the north and other parts of Iran. Finally, it is highly recommended to separate climate impacts from anthropogenic impacts on extreme hydrological and climatic variables.

Supporting information

The following material is available as part of the online article:

Figure S1. Flowchart of the methodology.

Figure S2. Regional probability distribution function of the annual maximum rainfall with all GCM models across the study area.

Table S1. Selected rainfall stations and their attributes.

Table S2. GCM models for this study.

References

Alexander L, Zhang X, Peterson T, Caesar J, Gleason B, Klein Tank A, *et al.* 2006. Global observed changes in daily climate extremes of temperature and precipitation. *J. Geophys. Res.* **111**: D05109.

Alijani B, O'Brien J, Yarnal B. 2008. Spatial analysis of precipitation intensity and concentration in Iran. *Theor. Appl. Climatol.* **94**: 107–124.

ASCE Task Committee on Application of Artificial Neural Networks in Hydrology. 2000. Artificial neural networks in hydrology. I: preliminary concepts. *J. Hydrol. Eng.* **5**(2): 115–123.

Coulibaly P, Dibike YB. 2005. Downscaling precipitation and temperature with temporal neural networks. *J. Hydrometeorol.* **6**: 483–496.

Fistikoglu O, Okkan U. 2011. Statistical downscaling of monthly precipitation using NCEP/NCAR reanalysis data for Tahtali river basin in Turkey. *J. Hydrol. Eng.* **16**: 157–164.

Frost AJ. 2007. *Australian Application of a Statistical Downscaling technique for Multi-site Daily Rainfall: GLIMCLIM*. MODSIM: Auckland. http://www.mssanz.org.au/MODSIM07/papers/10_s61/AustralianApplication_s61_Frost_.pdf (accessed 4 July 2017).

Goyal MK, Ojha CSP. 2012. Downscaling of surface temperature for lake catchment in an arid region in India using linear multiple regression and neural networks. *Int. J. Climatol.* **32**: 552–566.

Hegerl GC, Zwiers FW, Braconnot P, Gillett NP, Luo Y, Marengo Orsini JA, *et al.* 2007. Understanding and attributing climate change. In *Climate Change 2007: The Physical Science Basis. Contribution of Working Group I to the Fourth Assessment Report of the Intergovernmental Panel on Climate Change*, Solomon S, Qin D, Manning M, Chen Z, Marquis M, Averyt KB, *et al.* (eds). Cambridge University Press: Cambridge.

Hessami M, Gachon P, Ouarda TBMJ, St-Hilaire A. 2008. Automated regression-based statistical downscaling tool. *Environ. Modell. Softw.* **23**: 813–834.

Houghton JJ, Ding Y, Griggs DJ, Noguer M, van der Linden PJ, Dai X, *et al.* (eds). 2001. *What is GCM? IPCC (Intergovernmental Panel on Climate Change). IPCC Working Group I*. Cambridge University Press: Cambridge; 881.

Huang J, Zhang J, Zhang Z, Sun S, Yao J. 2012. Simulation of extreme precipitation indices in the Yangtze river basin by using statistical downscaling method (SDSM). *Theor. Appl. Climatol.* **108**: 325–343.

Huth R. 2004. Sensitivity of local daily temperature change estimates to the selection of downscaling models and predictors. *J. Clim.* **17**(3): 640–652.

Jeong DI, St-Hilaire A, Ouarda TBMJ, Gachon P. 2012a. Multisite statistical downscaling model for daily precipitation combined by multivariate multiple linear regression and stochastic weather generator. *Clim. Change* **114**(3-4): 567–591.

Jeong DI, St-Hilaire ATBMJ, Ouarda TBMJ, Gachon P. 2012b. Comparison of transfer functions in statistical downscaling models for daily temperature and precipitation over Canada. *Stochastic Environ. Res. Risk Assess.* **26**: 633–653.

Jeong DI, St-Hilaire A, Ouarda TBMJ, Gachon P. 2013. Projection of future daily precipitation series and extreme events by using a multi-site statistical downscaling model over the great Montréal area, Québec, Canada. *Hydrol. Res.* **44**(1): 147–168.

Li Z, Zheng FL, Liu W-Z, Jiang D-J. 2012. Spatially downscaling GCMs outputs to project changes in extreme precipitation and temperature events on the Loess Plateau of China during the 21st Century. *Global Planet. Change* **82–83**: 65–73.

McCulloch WS, Pitts W. 1943. A logical calculus of the ideas imminent in nervous activity. *Bull. Math. Biophys.* **5**: 115–133.

Millington N, Das S, Simonovic SP. 2011. The comparison of GEV, Log-Pearson type 3 and Gumbel distributions in the Upper Thames River watershed under Global Climate Models. Water Resources Research Report No. 077, The University of Western Ontario: London, Ontario, Canada; 52.

Raje D, Mujumdar PP. 2009. A conditional random field-based downscaling method for assessment of climate change impact on multisite daily precipitation in the Mahanadi basin. *Water Resour. Res.* **45**: W10404.

Sarhadi A, Burn DH, Johnson F, Mehrotra R, Sharma A. 2016. Water resources climate change projections using supervised nonlinear and multivariate soft computing techniques. *J. Hydrol.* **536**: 119–132.

Sarhadi A, Burn DH, Yang G, Ghodsi A. 2017. Advances in projection of climate change impacts using supervised nonlinear dimensionality reduction techniques. *Clim. Dyn.* **48**: 1329–1351. https://doi.org/10.1007/s00382-016-3145-0.

Schoof JT, Pryor SC. 2001. Downscaling temperature and precipitation: a comparison of regression-based methods and artificial neural networks. *Int. J. Climatol.* **21**: 773–790.

Shahriar Pervez MD, Henebry GM. 2014. Projections of the Ganges-Brahmaputra precipitation – Downscaled from GCM predictors. *J. Hydrol*. **517**: 120–134.

Tolika K, Anagnostopoulou C, Maheras P, Vafiadis M. 2008. Simulation of future changes in extreme rainfall and temperature conditions over the Greek area: a comparison of two statistical downscaling approaches. *Global Planet. Change* **63**: 132–151.

Tryhorn L, DeGaetano A. 2011. A comparison of techniques for downscaling extreme precipitation over the northeastern United States. *Int. J. Climatol.* **31**: 1975–1989.

Tue Vu M, Thannob Aribarg T, Siriporn Supratid S, Raghavan SV, Liong SY. 2016. Statistical downscaling rainfall using artificial neural network: significantly wetter Bangkok? *Theor. Appl. Climatol.* **126**: 453–467. https://doi.org/10.1007/s00704-015-1580-1.

Tumbo SD, Mpeta EM, Tadross M, Kahimba FC, Mbillinyi BP, Mahoo HF. 2010. Application of self-organizing maps technique in downscaling GCMs climate change projections for Same, Tanzania. *Phys. Chem. Earth.* **35**: 608–617.

